



HAL
open science

Influence of the acrylamide-based monomer on the sintering of ceramics shaped by gelcasting

Laurie Gaüzère, Clémence Besnard, Maël Pontoreau, Stéphane Carlotti,
Samuel Couillaud, Jean-Marc Heintz

► **To cite this version:**

Laurie Gaüzère, Clémence Besnard, Maël Pontoreau, Stéphane Carlotti, Samuel Couillaud, et al.. Influence of the acrylamide-based monomer on the sintering of ceramics shaped by gelcasting. Open Ceramics, 2023, 16, pp.100447. 10.1016/j.oceram.2023.100447. hal-04199163

HAL Id: hal-04199163

<https://hal.science/hal-04199163>

Submitted on 7 Sep 2023

HAL is a multi-disciplinary open access archive for the deposit and dissemination of scientific research documents, whether they are published or not. The documents may come from teaching and research institutions in France or abroad, or from public or private research centers.

L'archive ouverte pluridisciplinaire **HAL**, est destinée au dépôt et à la diffusion de documents scientifiques de niveau recherche, publiés ou non, émanant des établissements d'enseignement et de recherche français ou étrangers, des laboratoires publics ou privés.



Distributed under a Creative Commons Attribution - NonCommercial - NoDerivatives 4.0
International License



Influence of the acrylamide-based monomer on the sintering of ceramics shaped by gelcasting

Laurie Gaüzère^{a,b}, Clémence Besnard^b, Maël Pontoreau^a, Stéphane Carlotti^c,
Samuel Couillaud^b, Jean-Marc Heintz^{a,*}

^a Univ. Bordeaux, CNRS, Bordeaux INP, ICMCB, UMR 5026, F-33600, Pessac, France

^b Galtenco Solutions, Parc Scientifique Unitec 1, F-33600, Pessac, France

^c Univ. Bordeaux, CNRS, Bordeaux INP, LCPO, UMR 5629, F-33600, Pessac, France

ARTICLE INFO

Handling Editor: Dr P Colombo

Keywords:

Alumina
Gelcasting
Grain packing
Green microstructure
Sintering

ABSTRACT

Alumina ceramics were prepared by gelcasting, based on an *in-situ* polymerization that promotes the formation of homogeneous green ceramic parts and allows the preparation of complex shapes and/or large-size ceramics. The influence of the monomer on the sintering behaviour of alumina pellets has been studied by considering three acrylamide-based monomers, i.e. acrylamide (AM), methacrylamide (MAM) and dimethylacrylamide (DMAA). Slurries with an alumina solid content of 50 vol% have been cast and pre-sintered pellets (1000 °C) with relative densities around 55% were obtained. These presintered pellets exhibit different granular packing, depending on the initial monomer used, as demonstrated by X-ray tomography, SEM and Hg porosimetry analyses. This results in significant differences in sintering behaviour, giving rise to very different final densities after 1 h sintering at 1530 °C: from 88% to 98%. This behaviour is described in terms of shrinkage rate, linked to the granular packing induced by the gelation process.

1. Introduction

Ceramic materials are renowned for their high-temperature properties (chemically inertness, temperature resistance) and hardness. Machining dense ceramics is therefore very expensive. That explains why many works have been undertaken to develop net-shape processes that enable the production of parts with complex shapes. The best known are injection moulding [1], extrusion [2] and now additive manufacturing [3]. Another process, developed and patented in the 90s at Oak Ridge National Laboratory [4], is also noteworthy: gelcasting [5–7].

Actually, gelcasting makes it possible to obtain high quality ceramic parts with complex shapes and large dimensions. The principle of this process is based on the preparation of a suspension loaded with a ceramic powder, to which a monomer [8] and a cross-linking agent are added. After the casting and due to an initiator, these organic compounds will generate a 3D polymeric network [9], thereby freezing the ceramic suspension and ensuring a homogeneous and optimized packing of the grains.

This process has many advantages. First, high powder loadings (>50

vol%) can be achieved, reducing the shrinkage [10] during the drying step [11–13] and thus limiting the occurrence of stresses during this critical stage. Second, the suspension contains a low amount of organic compounds (≈ 3 wt%), which simplifies the debinding process. Third, various materials can be used for the design of the moulds, such as PVA [14], PVB [15], metal [16], wax [17] etc ..., that are reusable and low cost. Fourth, the samples obtained by gelcasting have a high green mechanical resistance, allowing for machining or modifications at a reduced costs at this stage [18]. Lastly, this method is applicable to ceramic powder [19–23], metallic powders [24,25], or polymers [26] which makes this process generic for the preparation of green materials.

In the literature related to gelcasting, acrylamide (AM) was the first monomer to be used [4,5,27]. It has been widely used in many works, including recently [28,29]. However, due to the toxic character of this compound, other acrylamide monomers have been considered such as methacrylamide (MAM) [16,30,31], dimethylacrylamide (DMAA) [32–36]. In the same way, acrylate monomers such as hydroxyethyl methacrylate (HEMA) [37], hydroxyethyl acrylate (HEA) [38,39], carboxyethyl acrylate (CEA) [40], diglyceryl acrylate (DGA) [41] or acrylic acid-based systems [42,43] were studied. For most of these monomers,

* Corresponding author, ICMCB-CNRS, 87 Av du Dr Schweitzer, 33600, Pessac, France.

E-mail address: jean-marc.heintz@icmcb.cnrs.fr (J.-M. Heintz).

<https://doi.org/10.1016/j.oceram.2023.100447>

Received 21 July 2023; Received in revised form 28 August 2023; Accepted 29 August 2023

Available online 3 September 2023

2666-5395/© 2023 The Authors. Published by Elsevier Ltd on behalf of European Ceramic Society. This is an open access article under the CC BY-NC-ND license (<http://creativecommons.org/licenses/by-nc-nd/4.0/>).

the same cross-linking agent has been commonly used, *i.e.* methyl-enebisacrylamide (MBAM). One should also mention that other non-toxic and natural gelling systems have been largely studied as for example agar, ISOBAM™ ... A well-documented review is proposed in Ref. [44]. As a general concern, the effect of the nature of the monomer on the gelcasting process has been investigated. Ortega et al. [8] compared different monomer systems for the gelcasting of foams. Pietrzak et al. [41] developed a new monomer to improve the properties of the ceramic suspensions and the sintered bodies. Hong et al. [23] studied the fabrication of ZrB₂-SiC ceramic composites, focusing their work on the influence of hydrogel characteristics on the mechanical properties of the sintered composites. Nevertheless, no study has yet been proposed to investigate the influence of acrylamide-based monomers on the microstructure of the obtained green compacts and on the subsequent sintering process. It is well known that the green microstructural characteristics, particularly grain packing and homogeneity, are of primary importance for densification [45]. When it comes to gelcasting, the question of the grain arrangement resulting from the suspension polymerization arises. Considering the same family of monomers, it is possible to produce green pellets under similar chemical and physical conditions that feature slightly different microstructures, resulting in varying sintering trajectories. This paper, therefore, presents a comparative study on the sintering of gelcast alumina using three distinct acrylamide monomers.

2. Experimental

2.1. Materials

All experiments conducted in this work were carried out using an α -alumina powder (purity >99.84 wt%, P172LSB, Alteo, France) with a theoretical density (d_{th}) of 3.97 g cm⁻³. The main impurities present in this powder are presented in Table 1 and the median particle size in volume is $d_{50} = 0.4 \mu\text{m}$. This value is in good agreement with the average particle size that can be observed in the SEM micrograph, given in Fig. 1.

The three tested monomers were acrylamide (AM: C₃H₅NO, >98%, Alfa Aesar, USA), methacrylamide (MAM: C₄H₇NO, >98%, TCI, Japan), and N,N'-dimethylacrylamide (DMAA: C₅H₉NO, stabilized with Mequinol (MEHQ), >99%, TCI, Japan). N,N'-methylenebisacrylamide (MBAM: C₇H₁₀N₂O₂, 97%, ThermoScientific, USA) was the cross-linking agent. To obtain a high solid loading and a high stability suspension, an ammonium polyacrylate dispersant was added (Dolapix CE64, Zschimmer&Schwarz, Germany). A plasticizer, (PEG 400: poly(ethylene glycol) 400, H(OCH₂CH₂)_nOH, ThermoScientific, USA) was also added to improve the drying behaviour of the samples [46]. Finally, ammonium persulfate (APS: (NH₄)₂S₂O₈, 98%, Alfa Aesar, USA) was used to initiate the polymerization. The semi-developed formulae of the resulting polymers are shown in Fig. 2, according to the initial monomer used.

2.2. Sample preparation

The gelcasting process is described in Fig. 3 and was the same for the three types of sample, as follows. First, a premix solution was prepared, containing the monomer, the cross-linking agent (MBAM), the dispersant (CE64) and the plasticizer (PEG 400). The same proportions were used for all slurries studied. Monomer content was 15 wt%, based on deionized water. MBAM to monomer ratio was 1/6. The amount of CE64 was 0.35 wt%, based on alumina powder and the amount of PEG 400 was 2.5 wt%, based on deionized water. All these compounds were

Table 1

Chemical composition of P172LSB alumina powder (Alteo data sheet).

Al ₂ O ₃	Na ₂ O	CaO	SiO ₂	Fe ₂ O ₃	MgO
99.84 wt%	400 ppm	210 ppm	295 ppm	180 ppm	500 ppm

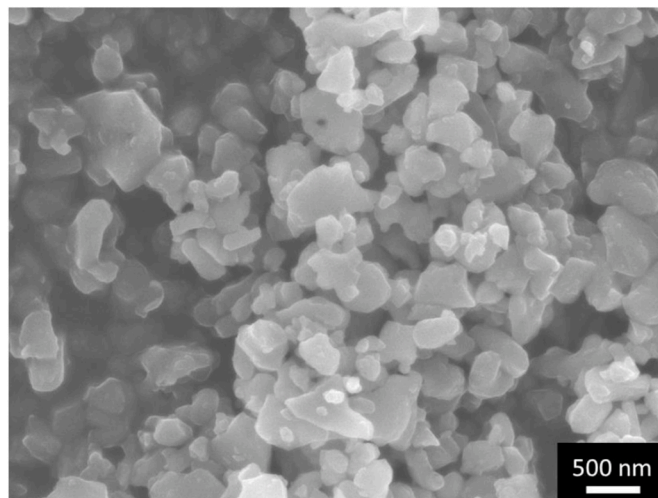


Fig. 1. SEM micrograph of the as-received α -alumina powder.

dissolved in deionized water. The alumina powder was then added with a solid load of 50 vol%. The slurry was then ball-milled for 24 h. The stability of the suspensions was checked. Their zeta potential was close and always greater than -30 mV at the working pH (pH = 9). The APS initiator was added after degassing the slurry, which was cast in 3D-printed plastic moulds. Following gelation at 60 °C, the samples were demoulded and subsequently dried, using an osmotic drying process in a liquid bath [47–49].

Dried bodies were then debinded at 600 °C for 1 h under air, with a heating rate of 0.5 °C/min. It was previously verified by thermogravimetric analysis (SetsysEvo, SETARAM, USA) that all organics were decomposed at 600 °C. The debinding cycle was followed by a pre-sintered stage, done in the same furnace, at 1000 °C for 1 h, under air, with a heating rate of 2 °C/min. This stage was added so that necks were created between grains and thus ensured mechanical strength to the samples. For sintering studies, the pre-sintered pellets (20 mm in height and 20 mm in diameter) were finally heat treated at 1530 °C for 1 h or 3 h in air, with a heating ramp of 10 °C/min. Some samples were also removed during the heating stage and air-quenched from 1420 °C.

2.3. Methods and characterizations

Debinding and sintering heat treatments were carried out in furnaces designed by Galtenco Solutions, which allow very precise control of the heating rate and the temperature in each part of the furnace [50,51]. Dilatometry measurements (DIL 402 C, NETZSCH, Germany) were conducted with a 10 °C/min heating ramp until 1475 °C (maximum temperature of the dilatometer) for 10 min on 5 × 5 × 5 mm³ pre-sintered samples. The relative densities of pre-sintered samples were obtained from mass and geometric measurements. Relative densities of sintered and air-quenched samples were determined by Archimedes' method in deionized water. These results are obtained from at least four pellets per sample type. The granular homogeneity of the pre-sintered pellets was investigated by X-ray tomography. These analyses were carried out (V|tome|X S, General Electric, USA) with the following experimental parameters: 0.1 mm Cu filter, U = 100 kV, I = 250 μA , exposure time 1 s, average of 3 images per projection, 2000 projections, voxel size 5 μm . In every case, 3D volumes were reconstructed from the collected radiographs using a filtered back projection Feldkamp-algorithm. To avoid experimental variations in X-ray absorption from one experiment to another, all samples were measured in a single run. Image analyses were then performed using the free and open-source Fiji software [52]. Pore size distributions of the presintered samples were determined by a mercury intrusion porosimeter (AutoPore IV, Micrometrics, USA). Microstructures of pre-sintered, air-quenched, and densified samples were

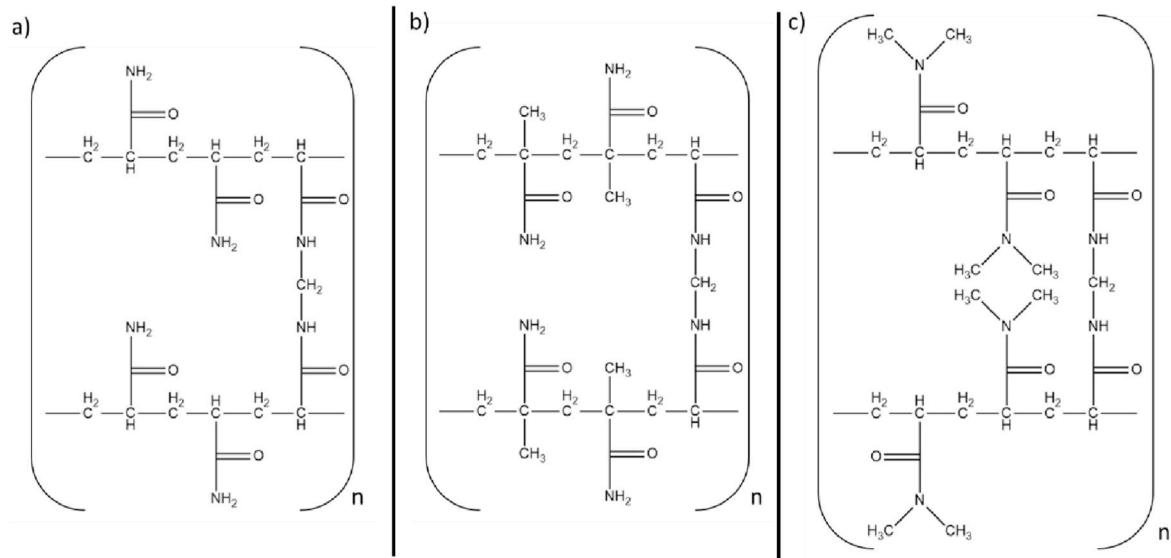


Fig. 2. Semi-developed formulae of the different studied polymers, a) polyacrylamide (PAM), b) polymethacrylamide (PMAM) and c) polydimethylacrylamide (PDMAA).

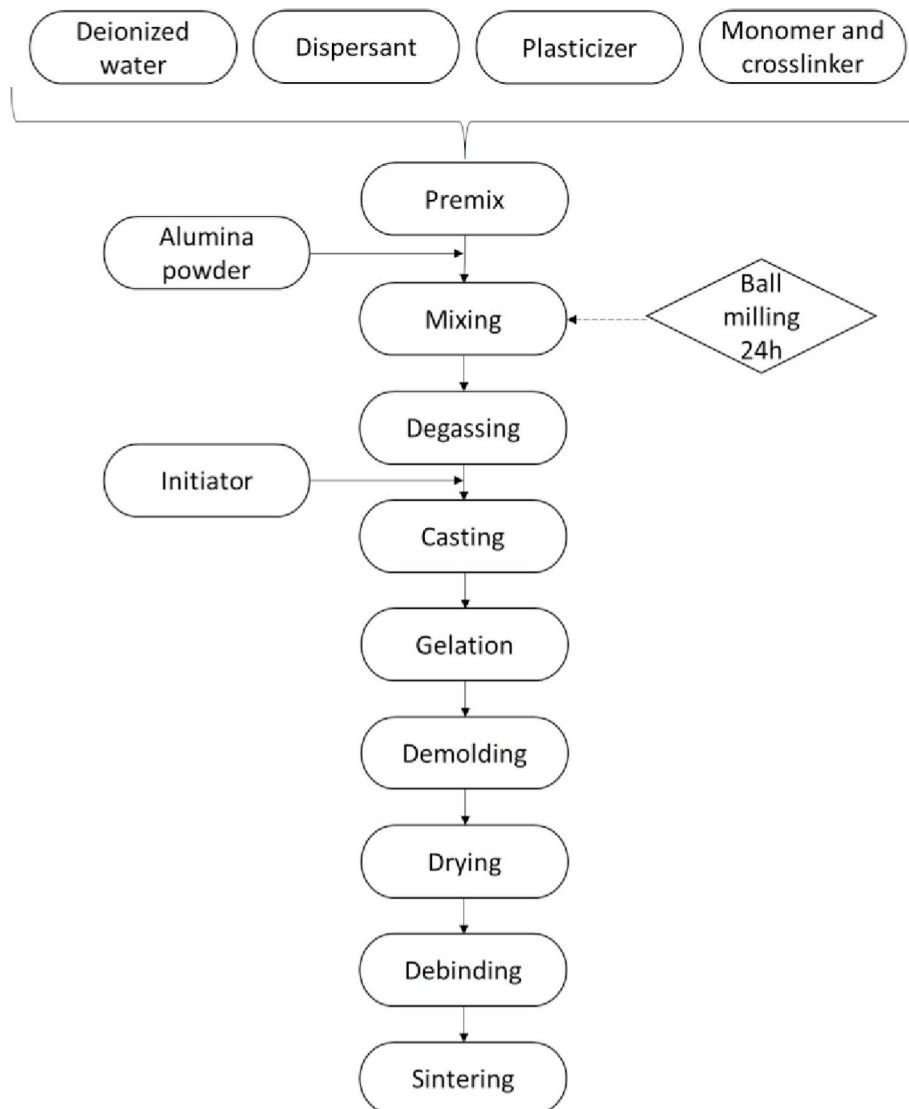


Fig. 3. Gelcasting flowchart.

observed using SEM (VEGA II SBH, TESCAN, Czech Republic). In order to determine the grain size, the sintered samples were polished using SiC discs and diamond suspensions down to $1/4 \mu\text{m}$. After polishing, the samples were thermally etched by performing an annealing treatment at $70 \text{ }^\circ\text{C}$ below the sintering temperature ($10 \text{ }^\circ\text{C}/\text{min}$ heating ramp and 10 min dwell time). The intercept method was used to determine the average intercept size (G) on SEM micrographs [53].

3. Results and discussions

3.1. Sintering

In the following, the samples studied are named according to the monomer used for gelcasting. Nevertheless, it should be reminded (Section 2.2) that no polymer, nor residual carbon was observed after the debinding and pre-sintering steps. Table 2 summarizes the relative

Table 2
Relative density (d) and grain size (G) of the pre-sintered and sintered samples.

Monomer	Pre-sintered	1530 °C-1 h		1530 °C-3 h	
	d (% d_{th})	d (% d_{th})	G (μm)	d (% d_{th})	G (μm)
AM	55.7 ± 1	96.2 ± 0.5	1.1 ± 0.1	98.2 ± 0.5	1.3 ± 0.2
MAM	54.9 ± 1	91.2 ± 0.5	1.1 ± 0.1	96.2 ± 0.5	1.3 ± 0.1
DMAA	53.6 ± 1	83.6 ± 0.5	0.9 ± 0.1	88.9 ± 0.5	1.1 ± 0.1

densities obtained before (pre-sintered state) and after sintering (1 h or 3 h at $1530 \text{ }^\circ\text{C}$), as well as the average grain size. A small difference is observed between the relative densities for the three pre-sintered pellets. This difference becomes large and significant after sintering at $1530 \text{ }^\circ\text{C}$ and increases with the sintering duration. The microstructures of the sintered samples are presented in Fig. 4. The porosity in the sintered samples appears quite different, depending on the initial monomer used. Indeed, the samples prepared with AM, Fig. 4 (a) and Fig. 4 (d), are almost dense whatever the sintering time. On the contrary, the samples made with DMAA, Fig. 4 (c) and Fig. 4 (f), show a significant amount of intergranular porosity, in agreement with the measured sintered densities that did not exceed 90% of the relative density. However, the increase in dwell time does not lead to appreciable grain growth, according to the G values provided in Table 2. Moreover, no abnormal growth is observed in SEM micrographs (Fig. 4).

3.2. Dilatometry

In order to explain the variations in densities found in Table 2, a dilatometry study was carried out on these samples, up to $1475 \text{ }^\circ\text{C}$. Fig. 5 (a) shows the evolution of the relative density as a function of temperature. Thanks to the gel casting process, there is no anisotropy of shrinkage (it was checked that the difference between radial and axial shrinkage was less than 1%) and the relative density can be deduced

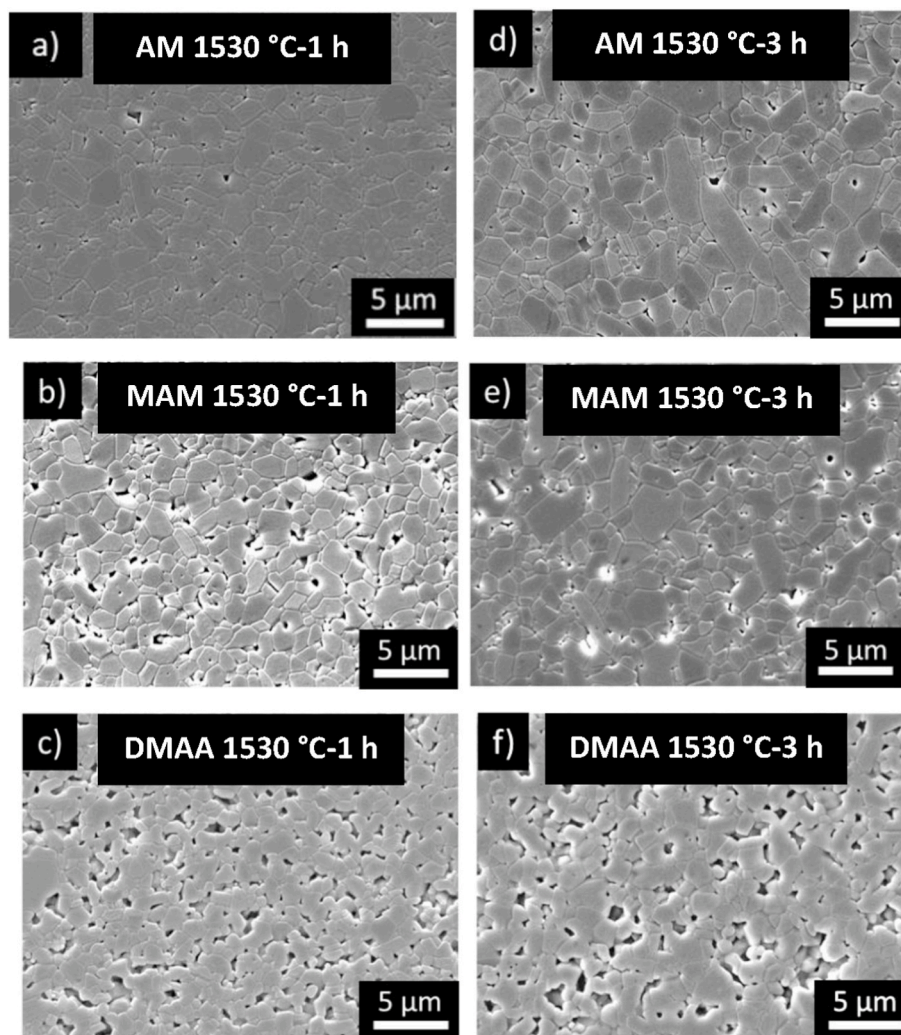


Fig. 4. SEM microstructures of samples sintered at $1530 \text{ }^\circ\text{C}$ for 1 h, initially gelcast with a) AM, b) MAM, c) DMAA and samples sintered at $1530 \text{ }^\circ\text{C}$ for 3 h, initially gelcast with d) AM, e) MAM and f) DMAA. All samples were polished and thermally etched.

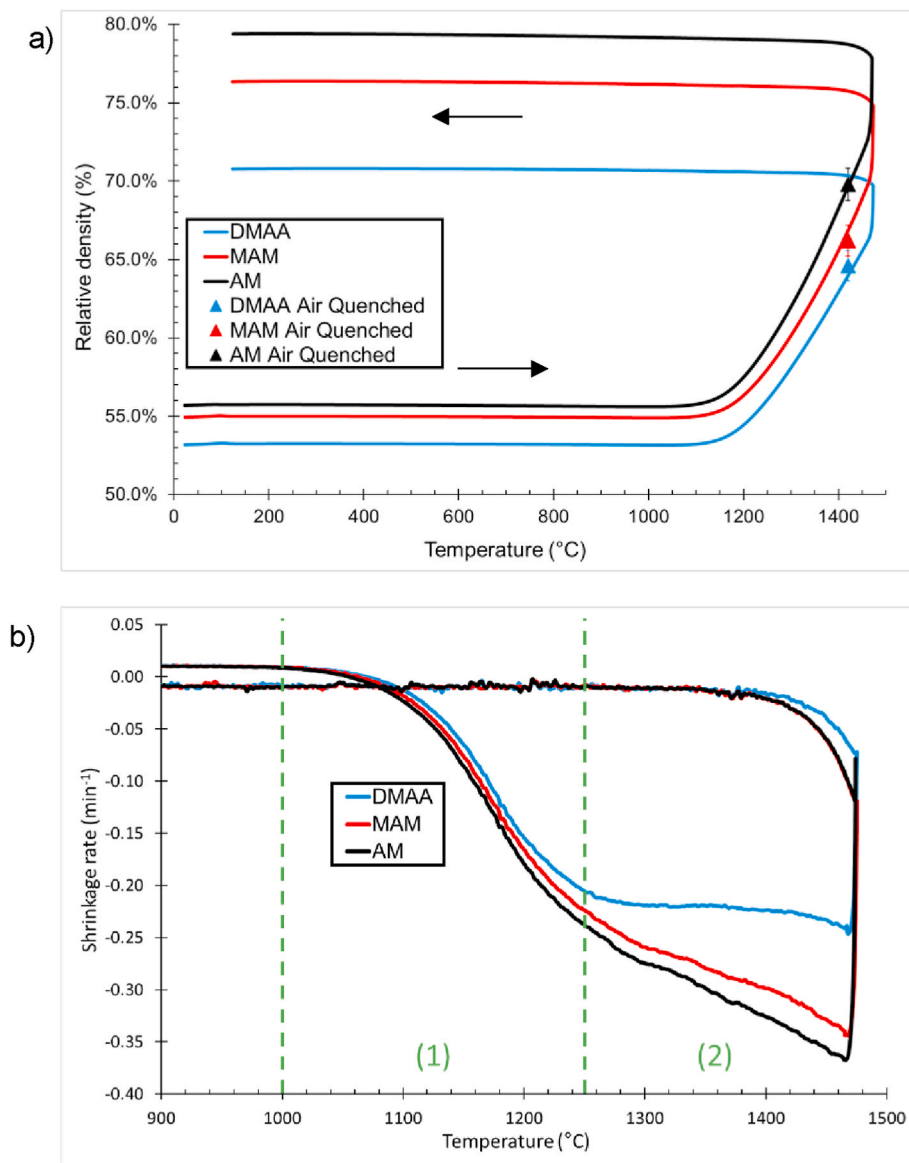


Fig. 5. a) Evolution of the relative density of pre-sintered samples as a function of temperature. The triangles correspond to densities measured on air-quenched ceramics. b) Shrinkage rate as a function of temperature.

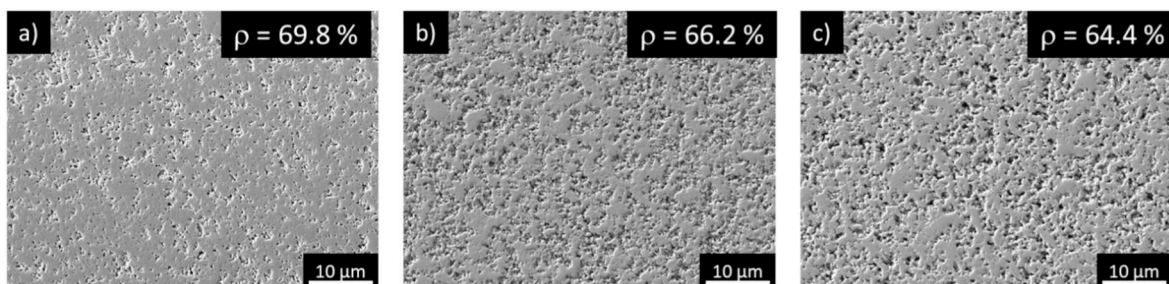


Fig. 6. SEM microstructures of quenched and polished samples, sintered up to 1420 °C and initially gelcast with the following monomers a) AM, b) MAM and c) DMAA.

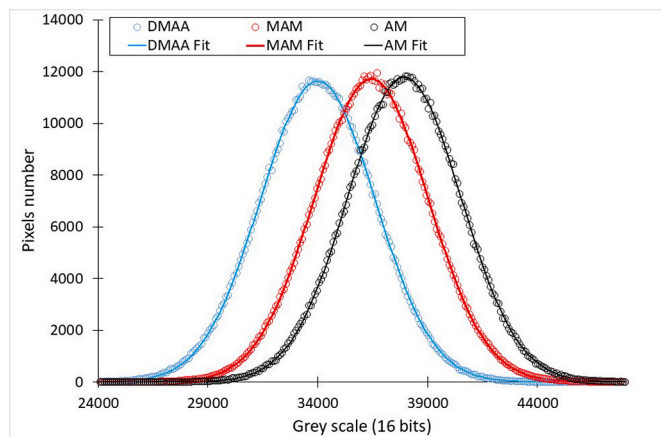


Fig. 7. Grayscale level distributions of pre-sintered samples, obtained by X-ray tomography.

from the shrinkage measurements according to [Equation \(1\)](#).

$$\rho_r = \frac{\rho_0}{\left(1 + \frac{\Delta l}{l_0}\right)^3} * 100 \quad (\text{Eq.1})$$

ρ_r , the relative density, ρ_0 , the pre-sintered density, $\frac{\Delta l}{l_0}$, the length variation during the dilatometry analysis.

For the three samples, the densification starts around 1100 °C and as the sintering temperature increases, the differences in relative density for the three samples become more pronounced. In particular, the AM sample showed a more significant change of slope than both the MAM and the DMAA samples. Furthermore, the evolution of the density during the stage at 1475 °C shows that DMAA sample densifies less than the other two. At the end of the dilatometric cycle, the final densities of the samples were 70.8%, 76.4% and 79.4% for the DMAA, MAM and AM samples respectively.

To determine more precisely the sintering behaviour of the three types of samples, the evolution of the shrinkage rate ($d(\Delta l/l_0)/dt$) as a function of temperature has been plotted ([Fig. 5 \(b\)](#)). This curve can be analysed by considering two temperature domains, characteristic of two different sintering stages. The first domain, (1), ranges from 1000 °C to approximately 1250 °C and corresponds to the start of sintering. This stage appears to be relatively similar for all three samples. However, a slight shift of the curves towards higher temperatures can be observed, related to a small difference in terms of onset of sintering. The lower the green (pre-sintered) relative densities, the higher the temperature at which sintering begins. Thus, the sintering of AM sample begins before that of the MAM and DMAA samples. The second domain, (2), starts at $T \sim 1250$ °C and a large difference in behaviour between the three types of samples can be seen. In particular, for the DMAA type pellets, the shrinkage rate remains nearly constant, contrary to the two other samples which, despite a change in slope from the previous domain, still

display an increasing shrinkage rate.

Air quenching at 1420 °C was also performed on the three types of samples in order to characterize their microstructure during the second sintering domain and their relative densities were also measured. This temperature has been chosen according to the shrinkage rate evolution ([Fig. 5 \(b\)](#)). The density values are plotted in [Fig. 5 \(a\)](#) and fit quite well with the dilatometry curves. The microstructures of these polished samples were analysed by SEM and are shown in [Fig. 6](#). At this temperature, the densification process has progressed significantly and notable differences could be observed. The AM pellet had a higher degree of sintering and less porosity than the other two samples, which is consistent with the measured densities. One can also notice that smaller pore sizes were present in AM compared to MAM and DMAA pellets.

3.3. Characterization of the pre-sintered pellets

As the densification depends directly on the initial grain packing when the same powder is used, characterization of the microstructure of the pre-sintered samples has been realised.

3.3.1. X-ray tomography (XRT)

An X-ray tomographic analysis was conducted to investigate at a macroscopic scale the granular homogeneity of the three pre-sintered samples. The resolution used was greater than the average grain size ($5 \mu\text{m} > 0.4 \mu\text{m}$), meaning each voxel represents a cluster of multiple grains, which will cause broad grey level distributions. Nonetheless, a homogeneous sample is likely to display a narrower grey level distribution than a more heterogeneous sample. The grey level distributions are shown in [Fig. 7](#). These distributions are symmetrical and can be well represented by a Gaussian function according to [Equation \(2\)](#) [54].

$$y = A * e^{-\frac{(x-\mu)^2}{2\sigma^2}} \quad (\text{Eq.2})$$

A is the peak height, μ is the peak position and σ is the full width at half maximum (FWHM).

The position (μ) of the peak of the histogram is related to the macroscopic density of the sample; the denser the material, the more the maximum will be shifted towards higher levels of grey (white). The full width at half maximum of the distribution (σ) can be used to characterize the homogeneity of the granular packing.

The data extracted from the fits of the grey level distribution curves, using the method of the least squares, are presented in [Table 4](#). These results indicate that the μ parameter increases from the DMAA type sample, to MAM and AM, which confirms the density measurements of the pre-sintered pellets, presented in [Table 2](#), where $d_{\text{DMAA}} < d_{\text{MAM}} < d_{\text{AM}}$.

[Table 4](#) also shows that the parameter σ evolves inversely to the parameter μ . That is, $\text{FWHM}_{\text{AM}} < \text{FWHM}_{\text{MAM}} < \text{FWHM}_{\text{DMAA}}$. This second observation reveals a difference in the homogeneity of the samples. The larger FWHM for the sample shaped from DMAA can be attributed to the presence of both denser and more porous zones than the other samples. This was confirmed by inspecting the fractures of the pre-

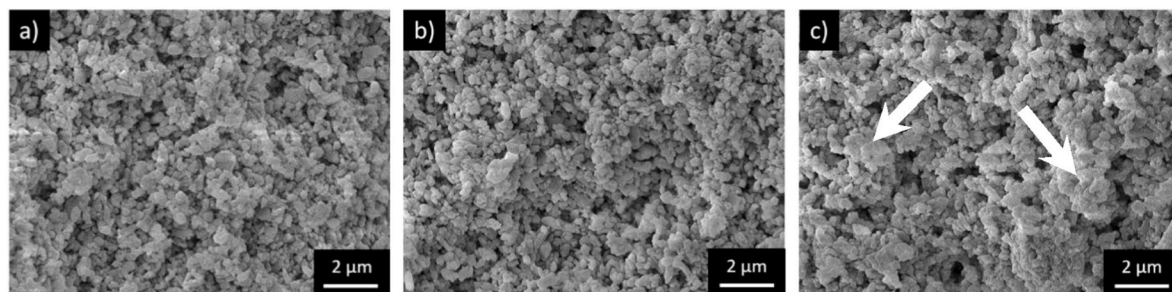


Fig. 8. SEM microstructures of fractures of pre-sintered samples, shaped with the following monomers: a) AM, b) MAM and c) DMAA. The white arrows highlight agglomerates.

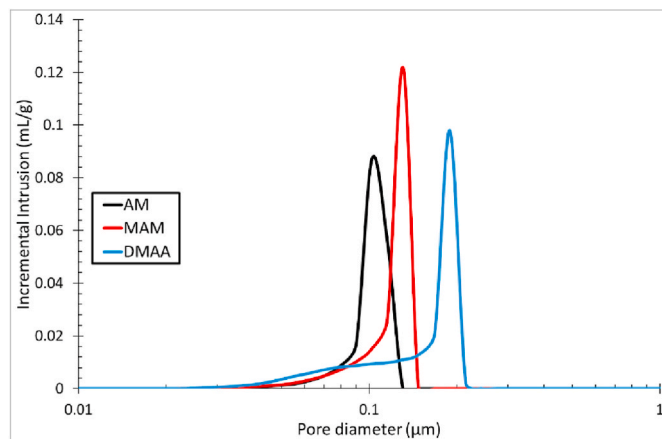


Fig. 9. Pore diameter distribution of pre-sintered samples, obtained from Hg-porosimetry.

Table 3
Porosity features of the pre-sintered samples.

	AM	MAM	DMAA
Porosity range (μm)	0.02–0.13	0.02–0.16	0.02–0.21
Mode of the distribution (μm)	0.10	0.13	0.19
Median pore diameter (μm)	0.11	0.14	0.19
Cumulative intrusion vol. (mL/g)	0.184	0.199	0.209

sintered samples (Fig. 8), which, particularly for the DMAA-type pellets, show the presence of agglomerates (marked by white arrows) composed of a few grains, and apparently larger porosities than in the other samples.

3.3.2. Hg-porosimetry

Fig. 9 shows the pore size distribution of the presintered pellets. The porosity is primarily of a macroporous type ($D_p > 50$ nm), although a small amount of mesoporosity ($2 \text{ nm} < D_p < 50$ nm) is also present in the case of DMAA. The size distribution of the pores is mainly monomodal for both AM and MAM samples, while that of DMAA has a significant peak foot on the side of the small pore sizes. Taking only the main mode (or the median of the distribution) into consideration, it is found that the smallest pore size is for AM, followed by MAM and DMAA (Table 3). Therefore, the DMAA has a wider porosity range than the two other pellets. The cumulative volume of mercury intrusion given in Table 3 also confirms the previous relative density measurements of pre-sintered materials, with lower porosity for AM type samples, followed by MAM and DMAA.

3.4. Discussion

The first sintering domain, identified below ~ 1250 °C on Fig. 5(b), can be attributed to the first stage of sintering [45], which is formation and growth of necks between particles. All three samples were made from the same P172LSB alumina powder, and so the formation of necks between the same types of particle, shaped in the same way (gelcasting), should exhibit the same kinetics - as was observed in Fig. 5(b). The slight differences in the onset sintering temperatures are likely due to

Table 4
Parameters characterizing the grey level distributions obtained by tomographic analysis of the 3 types of samples.

	AM	MAM	DMAA
A	$11,782 \pm 11$	$11,707 \pm 10$	$11,630 \pm 10$
μ	$37,937 \pm 3$	$36,432 \pm 3$	$34,000 \pm 3$
σ	2576 ± 3	2592 ± 3	2610 ± 3

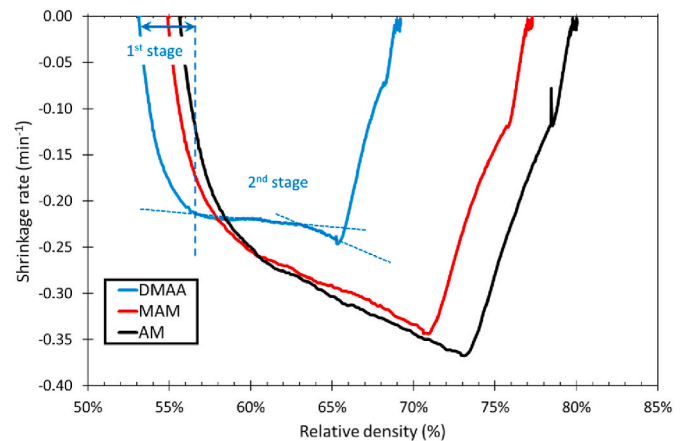


Fig. 10. Evolution of the shrinkage rate as a function of relative density for the 3 types of samples.

variations in the grain coordination number between the samples. Lower relative densities correspond to lower grain coordination numbers [45], which explains why the DMAA-type sample begins sintering at a slightly higher temperature than the MAM and AM samples. A way to confirm that domain (1) corresponds to the first stage of sintering is to express the shrinkage rate as a function of the relative density. Fig. 10 shows, for all curves, a clear change in slope that can be used to separate the previously identified domains (1) and (2) (this is only illustrated for the DMAA sample in Fig. 10). Domain (1) corresponds to an increase in density of about 3–5% for the three types of samples, a result which is expected for this stage.

The second domain is related to the densification of the granular packing obtained through the gelcasting process (Fig. 5 b). Although the gelation process produces homogeneous green compacts, heterogeneities in the grain packing (agglomerates, difference of porosity ...) cannot be entirely avoided. Indeed, X-Ray tomography and porosity measurements, presented above, demonstrate that the density and homogeneity of the granular packing of the green bodies can be slightly modified, according to the monomer used during the gelcasting process. It should be noted that these variations remain quite small compared to prior experiments displaying the effect of the initial density of the green compacts on their subsequent sintering [55,56]. It is well-documented in the literature that packing defects generate heterogeneities that favour the formation of dense regions surrounded by large pores, in other words, that generate different sintering rates within a same compact (differential sintering) [45]. Considering the two extreme samples (DMAA and AM), the microstructure characterizations show that these pre-sintered samples have different granular homogeneities (different grey level distributions in XRT) and pore sizes. The DMAA has a less homogeneous packing, a larger pore size, and a wider pore size distribution, resulting in lower densification rate than those of AM. Indeed, the shrinkage rate of DMAA pellets is almost constant for temperatures above 1250 °C (Fig. 5 b) and 10). Such a behaviour agrees quite well with the assumption of Zheng or German that suggested that a pore size less than half of the grain size is typically necessary to ensure densification [45,57]. DMAA has an initial median pore size close to half of the initial grain size of P172LSB powder ($D_p \sim \frac{d_{50}(\text{P172LSB})}{2}$), which is not the case of AM and MAM type samples. However, when sintering is proceeding, grain growth occurs, and in the case of DMAA, the pore size that should remain almost constant at the start of densification becomes lower than half of the grain size, resulting in improved densification. This can be seen in Fig. 10 where the DMAA shrinkage rate rises again when the relative density exceeds 63%. Then, the slope of this sample becomes similar to the slope of the two other samples.

The sintering trajectories analysed and discussed here are thus related to the microstructure of the green bodies, which is itself induced

by the nature of the monomer involved in the gelcasting stage. A first approach is to consider the hydrophilicity of the monomers and polymers. From the polymer (monomer) formulas given in Fig. 2, it appears that AM possesses terminal $-NH_2$ groups, MAM possesses $-CH_3$ and $-NH_2$ groups, while DMAA only presents $-CH_3$ groups. Methyl groups are known for their low affinity with water, whereas amine groups are hydrophilic. Viscosity measurements were performed on alumina slurries (before the addition of the initiator) as a function of the monomer used. The values obtained at a 10 s^{-1} shear rate were $\eta(\text{AM}) = 79\text{ mPa}\cdot\text{s}$ and $\eta(\text{MAM}) \sim \eta(\text{DMAA}) = 97\text{ mPa}\cdot\text{s}$. The suspensions containing DMAA and MAM exhibit slightly higher viscosity compared to those containing AM, suggesting that the presence of methyl groups does not promote suspension dispersion. Also, during gelation, the more polar character of the amine groups favours the establishment of hydrogen bonds with the surface of alumina grains, which are negatively charged under the conditions of suspension preparation ($\text{pH} = 9$). These hydrogen bonds between the polymer and the surface of alumina grains should promote the coating and dispersion of the grains within the polymer, thus improving the granular packing, finally observed in the pre-sintered samples. A less uniform microstructure is observed in the pellets shaped with the monomer containing more methyl groups. These hypotheses still require confirmation and are currently under investigation. They will be presented in an upcoming article.

4. Conclusion

This work demonstrates that the choice of the monomer in the gelcasting process is of primary importance to promote a high degree of homogeneity in the green compact, resulting in enhanced densification.

Alumina ceramics were shaped by gelcasting, considering three chemically related monomers of the acrylamide family, AM, MAM and DMAA. After debinding and pre-sintering heat treatments, a small difference in relative density has been pointed out, with higher values for AM type samples. After sintering at $1530\text{ }^\circ\text{C}$, a large difference in densification was observed, ranging from 88% for the DMAA sample to 98% for the AM sample. Through a dilatometry study, two different sintering domains were identified. The first one, similar for the 3 samples, was attributed to the first stage of sintering, i.e. formation and growth of necks between particles. The second one could be related to the grain packing formed during gelcasting. The granular homogeneity of the pre-sintered compact was characterized by X-ray tomography. It was shown that the use of DMAA monomer leads to a less homogeneous microstructure than with the two other monomers. Hg-porosimetry also showed that the median pore size as well as the amount of porosity within the pre-sintered pellets were slightly larger for DMAA compared to MAM and then to AM. These observations were confirmed by SEM analyses that show more agglomeration in the DMAA pre-sintered pellets. As a result, a slightly less homogeneous grain packing, including small agglomerates and/or larger porosities result in a large difference in final sintered density.

Finally, the homogeneity of the granular packing may be related to the varying hydrophilicity of the monomer. The formation of hydrogen bonds with the surface of alumina grains during slurry preparation and polymerization is likely to promote grain dispersion and thus packing when the polymer is removed.

Declaration of competing interest

The authors declare that they have no known competing financial interests or personal relationships that could have appeared to influence the work reported in this paper.

Acknowledgements

The authors would like to thank G. Hauss, from the PLACAMAT laboratory, for his great help during the X-Ray Tomography data

treatment, L. Lapuyade, from the LCTS laboratory, for the Hg-porosimetry measurement and the MATEIS laboratory for the discussions about the characterizations of the green parts by X-Ray tomography. This work was funded by the French National Agency of Research and Technology (ANRT) under contract number 2019/1751 and by the Nouvelle-Aquitaine region under contract number 10884920.

References

- [1] A. Zocca, P. Colombo, C.M. Gomes, J. Günster, Additive manufacturing of ceramics: issues, potentialities, and opportunities, *J. Am. Ceram. Soc.* 98 (2015) 1983–2001, <https://doi.org/10.1111/jace.13700>.
- [2] R. Ruprecht, T. Gietzelt, K. Müller, V. Piötter, J. Haubelt, Injection molding of microstructured components from plastics, metals and ceramics, *Microsyst. Technol.* 8 (2002) 351–358, <https://doi.org/10.1007/s00542-001-0153-7>.
- [3] I. Grida, J.R.G. Evans, Extrusion freeforming of ceramics through fine nozzles, *J. Eur. Ceram. Soc.* 23 (2003) 629–635, [https://doi.org/10.1016/S0955-2219\(02\)00163-2](https://doi.org/10.1016/S0955-2219(02)00163-2).
- [4] M.A. Janney, O.O. Omatete, U.S. Patent, Method for Molding Ceramic Powders Using a Water-Based Gel Casting, 5, 1991, p. 362, 028.
- [5] A.C. Young, O.O. Omatete, M.A. Janney, P.A. Menchhofer, Gelcasting of alumina, *J. Am. Ceram. Soc.* 74 (1991) 612–618, <https://doi.org/10.1111/j.1151-2916.1991.tb04068.x>.
- [6] O.O. Omatete, M.A. Janney, S.D. Nunn, Gelcasting: from laboratory Development toward industrial production, *J. Eur. Ceram. Soc.* 17 (1997) 407–413.
- [7] M.A. Janney, O.O. Omatete, C.A. Walls, S.D. Nunn, R.J. Ogle, G. Westmoreland, Development of low-toxicity gelcasting systems, *J. Am. Ceram. Soc.* 81 (2005) 581–591, <https://doi.org/10.1111/j.1151-2916.1998.tb02377.x>.
- [8] F.S. Ortega, P. Sepulveda, V.C. Pandolfelli, Monomer systems for the gelcasting of foams, *J. Eur. Ceram. Soc.* 22 (2002) 1395–1401, [https://doi.org/10.1016/S0955-2219\(01\)00486-1](https://doi.org/10.1016/S0955-2219(01)00486-1).
- [9] Bio-Rad, Acrylamide Polymerization – A Practical Approach, 2022. https://www.bio-rad.com/webroot/web/pdf/lsr/literature/Bulletin_1156.pdf.
- [10] A. Barati, M. Kokabi, M.H.N. Famili, Drying of gelcast ceramic parts via the liquid desiccant method, *J. Eur. Ceram. Soc.* 23 (2003) 2265–2272, [https://doi.org/10.1016/S0955-2219\(03\)00045-1](https://doi.org/10.1016/S0955-2219(03)00045-1).
- [11] A. Barati, M. Kokabi, N. Famili, Modeling of liquid desiccant drying method for gelcast ceramic parts, *Ceram. Int.* 29 (2003) 199–207, [https://doi.org/10.1016/S0272-8842\(02\)00106-2](https://doi.org/10.1016/S0272-8842(02)00106-2).
- [12] G.W. Scherer, Drying gels, *J. Non-Cryst. Solids* (1986) 199–225, [https://doi.org/10.1016/S0022-3093\(86\)80079-5](https://doi.org/10.1016/S0022-3093(86)80079-5).
- [13] G.W. Scherer, Correction of “Drying gels: 1. General theory,”, *J. Non-Cryst. Solids* (1987) 375–382, [https://doi.org/10.1016/S0022-3093\(87\)80056-X](https://doi.org/10.1016/S0022-3093(87)80056-X).
- [14] T. Tu, G. Jiang, SiC reticulated porous ceramics by 3D printing, gelcasting and liquid drying, *Ceram. Int.* 44 (2018) 3400–3405, <https://doi.org/10.1016/j.ceramint.2017.11.133>.
- [15] K. Liu, C. Zhou, F. Chen, H. Sun, K. Zhang, Fabrication of complicated ceramic parts by gelcasting based on additive manufactured acetone-soluble plastic mold, *Ceram. Int.* 46 (2020) 25220–25229, <https://doi.org/10.1016/j.ceramint.2020.06.313>.
- [16] R. Gillissen, J.P. Erauw, A. Smolders, E. Vanswijgenhoven, J. Luyten, Gelcasting, a near net shape technique, *Mater. Des.* 21 (2000) 251–257, [https://doi.org/10.1016/S0261-3069\(99\)00075-8](https://doi.org/10.1016/S0261-3069(99)00075-8).
- [17] S. Dhara, R.K. Kamboj, M. Pradhan, P. Bhargava, Shape forming of ceramics via gelcasting of aqueous particulate slurries, *Bull. Mater. Sci.* 25 (2002) 565–568, <https://doi.org/10.1007/BF02710552>.
- [18] S.D. Nunn, G.H. Kirby, Green machining of gelcast ceramic materials, *Ceram. Eng. Sci. Proc.* 17 (1996) 209.
- [19] H. Luo, P. Xiao, L. Huang, W. Hong, Dielectric properties of Cf-Si3N4 sandwich composites prepared by gelcasting, *Ceram. Int.* 40 (2014) 8253–8259, <https://doi.org/10.1016/j.ceramint.2014.01.023>.
- [20] Y. Yang, S. Shimai, Y. Sun, M. Dong, H. Kamiya, S. Wang, Fabrication of porous Al₂O₃ ceramics by rapid gelation and mechanical foaming, *J. Mater. Res.* 28 (2013) 2012–2016, <https://doi.org/10.1557/jmr.2013.170>.
- [21] J.-H. Eom, Y.-W. Kim, S. Raju, Processing and properties of macroporous silicon carbide ceramics: a review, *Journal of Asian Ceramic Societies* 1 (2013) 220–242, <https://doi.org/10.1016/j.jascer.2013.07.003>.
- [22] J. Xue, M. Dong, J. Li, G. Zhou, S. Wang, Gelcasting of aluminum nitride ceramics, *J. Am. Ceram. Soc.* 93 (2010) 928–930, <https://doi.org/10.1111/j.1551-2916.2009.03489.x>.
- [23] W. Hong, P. Hu, D. Zhang, M. Xie, Y. Yang, S. Du, Fabrication of ZrB₂-SiC ceramic composites by optimized gel-casting method, *Ceram. Int.* 44 (2018) 6037–6043, <https://doi.org/10.1016/j.ceramint.2017.12.227>.
- [24] H.H. Liang, F. Wang, K.Y. Jiang, Experimental study on drying process of green body in gelcasting of metal part, *Appl. Mech. Mater.* 217–219 (2012) 1894–1898, <https://doi.org/10.4028/www.scientific.net/AMM.217-219.1894>.
- [25] J. Stampfl, H.-C. Liu, S.W. Nam, K. Sakamoto, H. Tsuru, S. Kang, A.G. Cooper, A. Nickel, F.B. Prinz, Rapid prototyping and manufacturing by gelcasting of metallic and ceramic slurries, *Mater. Sci. Eng., A* 334 (2002) 187–192, [https://doi.org/10.1016/S0921-5093\(01\)01800-7](https://doi.org/10.1016/S0921-5093(01)01800-7).
- [26] A.G.A. Coombes, J.D. Heckman, Gel casting of resorbable polymers : 1. Processing and applications, *Biomaterials* 13 (1992).

- [27] J. Ma, Z. Xie, H. Miao, Y. Huang, Y. Cheng, W. Yang, Gelcasting of alumina ceramics in the mixed acrylamide and polyacrylamide systems, *J. Eur. Ceram. Soc.* 23 (2003) 2273–2279, [https://doi.org/10.1016/S0955-2219\(03\)00041-4](https://doi.org/10.1016/S0955-2219(03)00041-4).
- [28] Q. Yao, L. Zhang, H. Chen, P. Gao, C. Shao, X. Xi, L. Lin, H. Li, Y. Chen, L. Chen, A novel gelcasting induction method for YAG transparent ceramic, *Ceram. Int.* 47 (2021) 4327–4332, <https://doi.org/10.1016/j.ceramint.2020.09.266>.
- [29] A. Parsi, F. Golestani-Fard, S.M. Mirkazemi, The effect of gelcasting parameters on microstructural optimization of porous Si₃N₄ ceramics, *Ceram. Int.* 45 (2019) 9719–9725, <https://doi.org/10.1016/j.ceramint.2019.01.222>.
- [30] M. Potoczek, A catalytic effect of alumina grains onto polymerization rate of methacrylamide-based gelcasting system, *Ceram. Int.* 32 (2006) 739–744, <https://doi.org/10.1016/j.ceramint.2005.05.011>.
- [31] S. Dhara, P. Bhargava, Influence of nature and amount of dispersant on rheology of aged aqueous alumina gelcasting slurries, *J. Am. Ceram. Soc.* 88 (2005) 547–552, <https://doi.org/10.1111/j.1551-2916.2005.00122.x>.
- [32] S. Yin, S. Jiang, L. Pan, L. Guo, Z. Zhang, J. Zhang, X. Li, T. Qiu, J. Yang, Effects of solid loading and calcination temperature on microstructure and properties of porous Si₃N₄ ceramics by aqueous gelcasting using DMAA system, *Ceram. Int.* 45 (2019) 19925–19933, <https://doi.org/10.1016/j.ceramint.2019.06.250>.
- [33] S. Yin, L. Pan, X. Fang, Y. Li, Y. Li, Y. Feng, T. Qiu, J. Yang, Porous Si₃N₄ ceramics prepared by aqueous gelcasting using low-toxicity DMAA system: regulatable microstructure and properties by monomer content, *Ceram. Int.* 45 (2019) 9994–10003, <https://doi.org/10.1016/j.ceramint.2019.02.043>.
- [34] W. Wan, J. Yang, J. Zeng, T. Qiu, Gelcasting of fused silica glass using a low-toxicity monomer DMAA, *J. Non-Cryst. Solids* 379 (2013) 229–234, <https://doi.org/10.1016/j.jnoncrysol.2013.08.017>.
- [35] W. Wan, J. Yang, J. Zeng, L. Yao, T. Qiu, Effect of solid loading on gelcasting of silica ceramics using DMAA, *Ceram. Int.* 40 (2014) 1735–1740, <https://doi.org/10.1016/j.ceramint.2013.07.071>.
- [36] W. Wan, J. Yang, J. Zeng, L. Yao, T. Qiu, Aqueous gelcasting of silica ceramics using DMAA, *Ceram. Int.* 40 (2014) 1257–1262, <https://doi.org/10.1016/j.ceramint.2013.06.048>.
- [37] K. Cai, Y. Huang, J. Yang, Alumina gelcasting by using HEMA system, *J. Eur. Ceram. Soc.* 25 (2005) 1089–1093, <https://doi.org/10.1016/j.jeurceramsoc.2004.04.024>.
- [38] L.G. Ma, Y. Huang, J.L. Yang, H.R. Le, Y. Sun, Control of the inner stresses in ceramic green bodies formed by gelcasting, *Ceram. Int.* 32 (2006) 93–98, <https://doi.org/10.1016/j.ceramint.2004.12.011>.
- [39] A. Wieclaw-Midor, A. Wicinska, P. Szafran, Surface modification of alumina powder to prevent exfoliation of samples fabricated by gelcasting, *J. Ceram. Sci. Technol.* 9 (2018), <https://doi.org/10.4416/JCST2018-00008>.
- [40] E. Pietrzak, P. Wicinska, M. Szafran, 2-carboxyethyl acrylate as a new monomer preventing negative effect of oxygen inhibition in gelcasting of alumina, *Ceram. Int.* 42 (2016) 13682–13688, <https://doi.org/10.1016/j.ceramint.2016.05.166>.
- [41] E. Pietrzak, P. Wicinska, M. Poterala, M. Szafran, Diglyceryl acrylate as alternative additive dedicated to colloidal shaping of oxide materials – synthesis, characterization and application in manufacturing of ZTA composites by gelcasting, *J. Eur. Ceram. Soc.* 39 (2019) 3421–3432, <https://doi.org/10.1016/j.jeurceramsoc.2019.01.048>.
- [42] K. Prabhakaran, C. Pavithran, Gelcasting of alumina from acidic aqueous medium using acrylic acid, *J. Eur. Ceram. Soc.* 20 (2000) 1115–1119, [https://doi.org/10.1016/S0955-2219\(99\)00244-7](https://doi.org/10.1016/S0955-2219(99)00244-7).
- [43] M. Kokabi, A.A. Babaluo, A. Barati, Gelation process in low-toxic gelcasting systems, *J. Eur. Ceram. Soc.* 26 (2006) 3083–3090, <https://doi.org/10.1016/j.jeurceramsoc.2005.08.020>.
- [44] L. Montanaro, B. Coppola, P. Palmero, J.-M. Tulliani, A review on aqueous gelcasting: a versatile and low-toxic technique to shape ceramics, *Ceram. Int.* 45 (2019) 9653–9673, <https://doi.org/10.1016/j.ceramint.2018.12.079>.
- [45] R.M. German, *Sintering Theory and Practice*, John Wiley & Sons Inc, Wiley-Interscience, 1996.
- [46] M. Trunec, P. Stastny, J. Kastyl, Defect-free drying of large fine-particle zirconia compacts prepared by gelcasting method, *J. Eur. Ceram. Soc.* 42 (2022) 7180, <https://doi.org/10.1016/j.jeurceramsoc.2022.08.011> –7186.
- [47] M.A. Janney, J. Kiggans Jr., US patent, O. Method of drying articles 5 (1999) 493, 885.
- [48] M. Trunec, Osmotic drying of gelcast bodies in liquid desiccant, *J. Eur. Ceram. Soc.* 31 (2011) 2519–2524, <https://doi.org/10.1016/j.jeurceramsoc.2011.02.015>.
- [49] N. Somers, *Dopages de phosphate tricalcique beta et mise en forme de macroporeux par robocasting*, PhD defence, Polytechnique Hauts-De-France, 2021.
- [50] A. Allemand, C. Guerin, C. Besnard, R. Billard, Y. Le Petitcorps, A comparison between a new ultra fast pressureless sintering (UFPS) technology and spark plasma sintering (SPS) for barium AluminoSilicate metastable phase, *J. Eur. Ceram. Soc.* 41 (2021) 1524–1529, <https://doi.org/10.1016/j.jeurceramsoc.2020.09.054>.
- [51] I. Cornu, M. Cheype, M. Baudier-Pons, J.-F. Léon, S. Couillaud, F. Rossignol, J.-M. Heintz, Pixelated sintering of α -Al₂O₃, *J. Eur. Ceram. Soc.* (2022) 5885–5892, <https://doi.org/10.1016/j.jeurceramsoc.2022.06.007>.
- [52] J. Schindelin, I. Arganda-Carreras, E. Frise, V. Kaynig, M. Longair, T. Pietzsch, S. Preibisch, C. Rueden, S. Saalfeld, B. Schmid, J.-Y. Tinevez, D.J. White, V. Hartenstein, K. Eliceiri, P. Tomancak, A. Cardona, Fiji: an open-source platform for biological-image analysis, *Nat. Methods* 9 (2012) 676–682, <https://doi.org/10.1038/nmeth.2019>.
- [53] H. Abrams, Grain size measurement by the intercept method, *Metallography* 4 (1971) 59–78, [https://doi.org/10.1016/0026-0800\(71\)90005-X](https://doi.org/10.1016/0026-0800(71)90005-X).
- [54] H. Guo, A simple algorithm for fitting a Gaussian function, in: R.G. Lyons (Ed.), *Streamlining Digital Signal Processing*, John Wiley & Sons, Inc., Hoboken, NJ, USA, 2012, pp. 297–305, <https://doi.org/10.1002/9781118316948.ch31>.
- [55] J. Zhao, M.P. Harmer, Effect of pore distribution on microstructure development: I, Matrix pores, *J. Am. Ceram. Soc.* 71 (1988) 113–120.
- [56] T.-S. Yeh, M.D. Sacks, Effect of green microstructure on sintering of alumina, *Ceramic Transparent* 7 (1990) 309.
- [57] J. Zheng, J.S. Reed, Effects of particle packing characteristics on solid-state sintering, *J. Am. Ceram. Soc.* 72 (1989) 810–817.